Green Chemistry

Understanding Lignin Micro- and Nanoparticle Nucleation and Growth in Aqueous Suspensions by Solvent Fractionation

Journal:	*Green Chemistry*
Manuscript ID	GC-ART-10-2020-003632.R1
Article Type:	Paper
Date Submitted by the Author:	15-Dec-2020
Complete List of Authors:	Zwilling, Jacob; North Carolina State University, Forest Biomaterials Jiang, Xiao; North Carolina State University, Forest Biomaterials; NC State University Zambrano, Franklin; North Carolina State University, Forest Biomaterials Venditti, Richard; North Carolina State University, Forest Biomaterials Department Jameel, Hasan; North Carolina State University, Forest Biomaterials Velev, Orlin; North Carolina State University, Chemical Biomolecular Engineering Rojas, Orlando; Aalto University, Bioproducts and Biosystems, School of Chemical Engineering; University of British Colombia, Bioproducts Institute, Chemical & Biological Engineering, Chemistry, and Wood Science Gonzalez, Ronalds; North Carolina State University, Forest Biomaterials

ARTICLE

Understanding Lignin Micro- and Nanoparticle Nucleation and Growth in Aqueous Suspensions by Solvent Fractionation

Received 00th January 20xx,
Accepted 00th January 20xx

DOI: 10.1039/x0xx00000x

Jacob D. Zwilling[a], Xiao Jiang[a], Franklin Zambrano[a], Richard Venditti[a*], Hasan Jameel[a], Orlin D. Velev[b], Orlando J. Rojas[c], and Ronalds Gonzalez[a*]

There have been many recent advances toward developing sustainable, micro- and nanoscale materials from biobased resources such as lignin to further strengthen the bioeconomy. It is critical to study the factors affecting nucleation and growth mechanisms, as well as stability of lignin micro-and nanoparticles (LPs) to further enhance the development of such materials. However, there remains a gap in the literature examining the many interactions present during LP formation. These interactions vary with the chemical compostion and molecular weight distribution of different kraft lignin (KL) fractions. To examine the composition of different lignin fractions, KL can be fractionated using water-miscble organic solvents of different polarities such as tetrahydrofuran (THF), acetone, and ethanol. Herein, we show that the micro- and nanoparticles formed from each lignin fraction exhibit significant differences in their size (50-300 nm), particle aggregation and fusion propensity, and spherical morphology in aqueous suspensions. These differences are proposed to be due to the solvent-lignin-water interactions related to molecular weight and functional groups of the lignin fractions and solvent/water polarity. Another factor affecting the nucleation and growth of LPs is the lignin concentration. The LPs formed at low lignin concentrations exhibit a larger average particle size compared to the LPs formed at higher lignin concentrations due to the aggregation and fusion of the small particles. These results will allow for a stronger foundation in understanding the nucleation and growth of LPs when attempting to develop value-added applications for kraft lignin.

Introduction

Lignin micro- and nanoparticles have had heightened interest in the past decade in the attempt to enhance and apply lignin, a by-product of the pulp and paper industry, to more valuable applications. Applications of lignin have been investigated for close to 70 years, and yet the most practical use of this biopolymer is to combust it for energy and steam production. In the present work, softwood lignin was examined. Softwood lignin results from the polymerization, *in vivo*, of predominantly one of three monolignols, namely guaiacyl (G-unit), along with small amounts of *p*-hydroxyphenyl (H-unit).[1,2]

Kraft lignin (KL) has a significantly different structure than native lignin due to the harsh alkaline treatment during pulping. This includes the generation of a large number of hydroxyl groups as a result of the cleavage of ether bonds.[3,4] Due to lignin's multi-functional groups, mainly phenolic hydroxyl, carboxyl, and aliphatic hydroxyl groups, a unique set of properties are revealed related to its UV light absorption[5,6], emulsion stabilization ability[7], antioxidant effects[5], chelation[8] and antimicrobial activity.[9,10] These properties invoke the potential for the development of eco-friendly, high-value products from lignin. Although KL has great potential for valorization, there has remained a lack of exploitation of such properties due to KL's challenges in product development. Commonly met challenges in the attempt to apply KL to value-added applications include its propensity to form large, amorphous aggregates, its lack of solubility in water, and immiscibility with many thermoplastic and thermosetting polymers.[11]

In order to improve the suitability of kraft lignin for high-value applications, it can be modified chemically[12], fractionated to form more homogeneous samples[13], or precipitated into spherical submicron particles for easier dispersion and improved features.[9,14,15] Unmodified KL tends to form large, irregular-shaped aggregates with a high degree of heterogeneity. Although mechanical treatment can make such aggregates smaller, morphological uniformity remains an issue. Transforming lignin into small, spherical particles has advantages over utilizing KL in solution form.[15] Smooth, spherical nanoparticles have intrinsic features such as enhanced electrostatic double layer repulsion for higher stability given the smooth surface[16,17], minimized surface energy from the spherical shape, and a high total surface area per unit mass derived from their small size.[17] They may be easily applied in low viscosity suspensions and can be used when extremely small features are desired.

[a] Department of Forest Biomaterials, North Carolina State University, 2820 Faucette Drive, Raleigh NC, 27695, United States.
E-mail: richardv@ncsu.edu, rwgonzal@ncsu.edu
[b] Department of Chemical Engineering, North Carolina State University, 911 Partner's Way, Raleigh NC, 27695
[c] Bioproducts Institute, Departments of Chemical & Biological Engineering, Chemistry, and Wood Science, 2360 East Mall, The University of British Columbia, Vancouver, BC V6T 1Z3, Canada
* Corresponding authors

Solvent shifting, or nanoprecipitation, is a common method to synthesize colloidal lignin suspensions by means of supersaturation.[18–24] Various procedures have been developed experimentally including the addition of a lignin solution into excess antisolvent[25], the addition of excess antisolvent into a lignin solution[22], and dialysis[23], which are respectively depicted in Fig. 1a-c. In previous papers, particle formation mechanisms of lignin under various solvent shifting methods have been investigated but there remains a gap of comparing resulting particle characteristics and behavior in aqueous suspensions formed from kraft lignin fractionated using different organic solvents.[17,21,23–28]

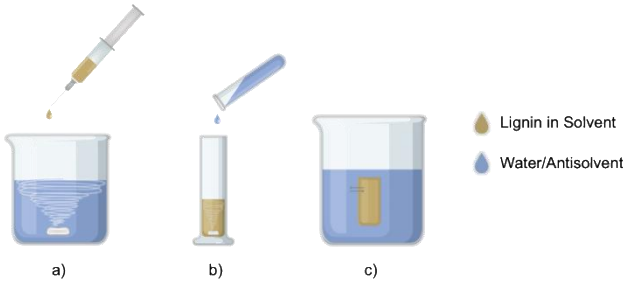

Fig. 1 Schematic of different solvent shifting methods including a) lignin solution-into-water, b) water-into-lignin solution, and c) dialysis of lignin solution with water.

Sipponen et al. determined that the formation of lignin particles in a common lignin solvent, ethanol, is dependent on solubility and ultimately molecular weight.[21] It was reported that the formation mechanism of LPs is kinetically-limited, where large molecular weight lignin fractions nucleate first and thereafter, smaller lignin molecules adsorb onto the surfaces of the nuclei.[21] Smaller, metastable soft particles may also form and can eventually fuse with the larger particles through a process called Ostwald ripening, contributing to the overall growth of the particles.[21] Leskinen et al. discussed a possible micro-emulsification mechanism where lignin molecules become entrapped within a droplet of solvent and as the antisolvent is added, the droplet constricts and eventually phase separates as the solvent concentration greatly decreases.[25]

Fractionation of KL through solvent extraction is a simple and effective method in homogenizing the lignin sample for LP fabrication.[24,25,29,30] Although, fractionation changes the MW distribution and chemical composition of the lignin used. Leskinen et al. found that the fractionation of lignin by increasing the concentration of water in THF as the solvating system yields a smaller particle size.[25] In contrast, Ma et al. showed that fractionating smaller molecular weight lignin molecules by using varying concentrations of ethanol and water prior to particle precipitation led to an inverse relationship between lignin molecular weight and particle size.[24] The results were attributed to the increase in the hydrophilic character of the lower molecular weight species, where hydrophobic forces tightly compacting the lignin particles are reduced.[24] It is worth noting that the lowest molecular weight fraction contained 67% of the starting lignin material, relating to a large degree of polydispersity.[24]

Previously reported studies have reported some relationships between molecular weight, chemical composition, and resulting particle size by fractionation techniques, but the fractionation techniques used prior to nanoprecipitation did not result in extensive separation of the low and medium molecular weight lignin fractions.[24,25,29,30] Thus, significant aggregation and metastability of lignin particles was not revealed or explored. Additionally, the effect of lignin concentration in solution on particle size has been briefly addressed as a general increasing trend with increasing concentration, but the metastability and aggregation propensity of LPs at low lignin concentrations has not been explored.

Herein, we show that fractionating KL with organic solvents of varying polarity (THF, acetone, and ethanol) results in distinct lignin fractions of approximately equal mass yields with significant differences in their molecular weight and chemical composition. The hydroxyl content and molecular weight of lignin fractions were characterized by ^{31}P-NMR and gel-permeation chromatography (GPC), respectively. The composition differences between the lignin fractions translates to a variability of colloidal behavior and resulting particle size when precipitated. The LPs' size and morphology was determined by dynamic light scattering (DLS) and transmission electron microscopy (TEM), respectively. Using both DLS and TEM particle size analysis techniques concomitantly allows for a greater understanding of the stability and colloidal behavior of the LPs. In addition to studying the effects of solvent fractionation on lignin particle formation, the effects of lignin concentration prior to precipitation are also examined. We propose that lignin particles must contain a high enough hydrophobicity to form discrete, compact, core-shell particles without exceeding a thermodynamically unfavorable surface free energy that may cause aggregation. The novelty of this work is related to describing the connection between the chemical composition of lignin, dissolved lignin concentration, and the colloidal interactions of LPs that result in formation of interparticle aggregates and particle fusion. The contribution of this work includes a deeper understanding of the nucleation and growth of LPs and their colloidal behaviour relating to aggregation propensity and/or particle fusion.

Experimental

Materials

Pine softwood kraft lignin (KL) extracted from black liquor via the LignoBoost method was used for all experiments. KL was acquired as an air-dried powder and the residual moisture was removed by vacuum oven drying for at least 24 hours prior to sampling. Acetone, ethanol, and tetrahydrofuran (1% BHT for stabilization) were acquired from Fisher Scientific (Waltham, MA, USA) and were reported as reagent grade (≥99% purity). Fractionated samples were centrifuged at 4000 RPM for 5 minutes using 50 mL Falcon centrifuge tubes (Corning, NY, USA) using an Eppendorf Centrifuge (Model: 5702). The transfer of

solutions and solvents was done using Eppendorf volumetric pipettes (500 µL-5 mL, 20 µL- 200µL). A plastic cuvette was used for dynamic light scattering measurements (Model: ZEN0040, Malvern Panalytical). Dialysis tubing with a molecular weight cut-off (MWCO) of 3500 Da was acquired from Fisher Scientific (Waltham, MA, USA).

Methods

To properly examine the effects of solvent fractionation of KL on LP synthesis, each lignin fraction must be analysed for their chemical structure and molecular weight distribution. This is critical for a better understanding of formed particle morphology, size, and colloidal behavior. Fig. 2 depicts the overall methodology of this work.

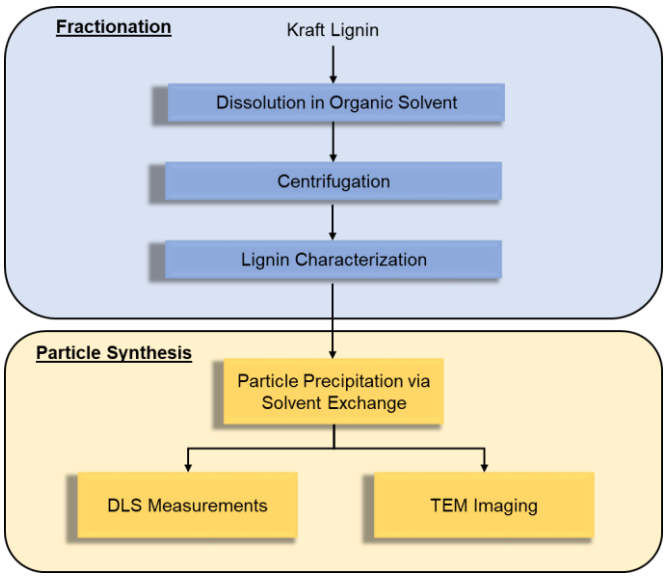

Fig. 2 Flowchart of lignin fractionation, characterization and particle synthesis.

Fractionation of Kraft Lignin

For preparing the lignin fractions, approximately 1 g of oven-dried KL was added to a 50 mL centrifuge tube along with 40 mL of anhydrous ethanol. The solution was mixed vigorously using a Fisher Scientific Digital Vortex Mixer for 60 seconds at 3,000 RPM to ensure maximum solubility. The mixture was then centrifuged for 5 minutes at 4,000 RPM. The supernatant was decanted and set aside for later use. In the same centrifuge tube, 40 mL of anhydrous acetone was added to the ethanol insoluble fraction and the previous steps were repeated. This process was repeated once more using anhydrous THF as the solvent. The THF insoluble fraction was discarded. This process is depicted schematically in Fig. 3. Each individual lignin fraction is hereby referred to as E-Frac, A-Frac, and T-Frac for lignin fractions soluble in ethanol, acetone, and THF respectively. Each lignin fraction was then dried by evaporating the solvent using a Büchi Rotovap R-100 followed by vacuum oven drying. Approximately 30 mg OD of each lignin fraction was set aside for GPC and 30 mg OD for NMR analysis. The remaining lignin from each fraction was then re-dissolved in its appropriate solvent to a concentration of 10 g/L. These lignin solutions were then used for LP synthesis

To characterize the KL soluble in acetone and THF without prior fractionation, approximately 1 g of oven-dried KL was added to 40 mL of both anhydrous acetone and THF separately. The solutions were then mixed using a vortex mixer for 60 seconds at 3,000 RPM to ensure maximum solubility. These solutions were centrifuged, and the insoluble portion was oven dried to determine solubility of the lignin in each solvent. The insoluble lignin fractions were discarded and only the soluble fractions were studied. The soluble portions are labelled as the combined acetone and ethanol soluble fractions (AE-Frac), and all three fractions combined, TAE-Frac. The solutions were then used for LP synthesis. The solubility of KL could be improved with each solvent by adding a portion of water during dissolution, but anhydrous solvents were used to clearly observe the effects of solvent-lignin-antisolvent interactions based on polarity and hydrogen bonding differences. Fig. 3 illustrates the labelling and description of each fraction.

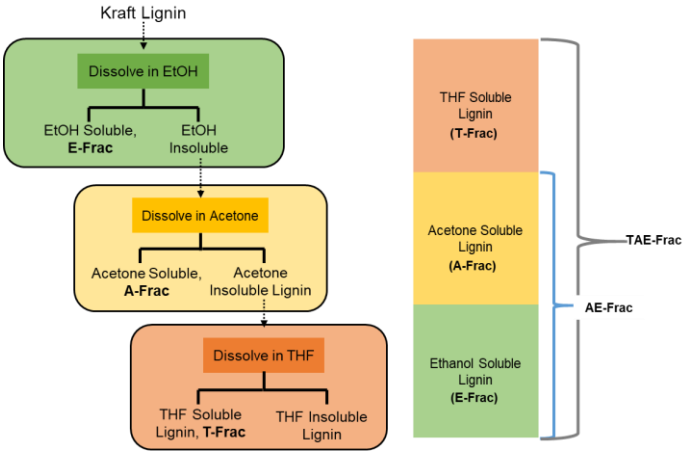

Fig. 3 Methodology of KL solvent fractionation and description of lignin fractions.

Molecular Weight Determination of Lignin Fractions by Gel-Permeation Chromatography

Gel permeation chromatography (GPC) was used to determine the average molecular weights and molecular weight distributions of the kraft lignin fractions. All lignin samples were acetylated prior to analysis to improve solubility in the mobile phase tetrahydrofuran (THF).[31] The analysis was performed using a Waters GPC instrument equipped with a UV detector (set at 280 nm) using (THF) as the eluent at a flow rate of 0.7 mL/min at 35 °C. A sample concentration of 1 mg/mL and an injection volume of 50 µL was used. Two ultra Styragel linear columns linked in series (Styragel HR 1 7.8 × 300 mm and Styragel HR 5E 7.8 × 300 mm) were used. A series of monodispersed polystyrene standards were used as calibration standards.[13]

Lignin Hydroxyl Group Content by ^{31}P-NMR Analysis

^{31}P-NMR analysis was performed to identify the various hydroxyl group contents of each lignin fraction. This analysis

was performed following the previously reported procedure.[32,33] The ^{31}P-NMR spectra were acquired using a Brüker 500 MHz spectrometer. Each peak was integrated to calculate the hydroxyl contents of each sample.

Derjaguin-Landau-Verwey-Overbeek (DLVO) Model of Lignin Particles

The energy of interaction as a function of interparticle distance was modelled using the DLVO theory of colloidal stability to determine the overall stability of the lignin particles with decreasing particle size. This model excludes non-DLVO forces beyond electrostatic repulsion and Van der Waals attractive forces. The following equations were used for the model derived by Israelachvilli[34]:

$$V_{rep} = \frac{R}{2} 9.22 \times 10^{-11} \tanh^2\left(\frac{\zeta_0}{103}\right) \exp(-\kappa D) \qquad (1)$$

$$V_{vdw} = -\frac{AR}{12D} \qquad (2)$$

$$V_{tot} = V_{rep} + V_{vdw} \qquad (3)$$

In Eqs. 1-3, V_{rep} is the potential energy of electrostatic repulsion at 25°C in an aqueous medium between two identical spheres with radii R, where ζ_0 is the surface potential approximated as the Zeta potential, κ is the Debye length, and D is the interparticle distance. V_{vdw} is the attractive Van der Waals potential energy, where A is the Hamaker constant of lignin approximated to be 1.7 x 10^{-20} J by Hollertz et al.[35]

Preparation of Kraft Lignin Particles

The synthesis of colloidal lignin particles was performed by first transferring 1 mL of the lignin fraction from each solvent solution to a 15 mL scintillation vial. After which, 9 mL of antisolvent (water or dilute NaOH solution) was quickly poured into the solution under rapid magnetic stirring (Fig. 1b). The colloidal suspensions are hereby referred to as TAE-LPs, AE-LPs, E-LPs, A-LPs, and T-LPs for particles precipitated from their respective lignin fractions TAE-Frac, AE-Frac, E-Frac, A-Frac, and T-Frac (Fig. 3). In order to obtain a concentration profile of particle size and morphology for each solvent system, dilutions of each lignin solution with the appropriate organic solvent were performed to obtain concentrations ranging from 0.5 to 10 g/L prior to antisolvent addition. Each suspension was dialyzed with DI water for 24 hours with Fisherbrand dialysis tubing (MWCO: 3500 Da) then further diluted with DI water to a final lignin concentration of 0.01 wt.%.

Dynamic Light Scattering

A Zetasizer Nano ZS instrument (Malvern Instruments Ltd.) was used for particle size analysis and ζ-potential of all samples. For particle size measurements, approximately 2 ml of the colloidal lignin suspension was added to a plastic cuvette (ZEN0040, Malvern, U.K) with lignin concentrations of 0.01 wt.% for each sample, within the concentration range advised by the manufacturer (Malvern Panalytical Ltd.). Particle size measurements were performed in duplicate at 25°C after an equilibration time of 120 seconds. The particle sizes are determined by an intensity weighted average (Z-average) of scattered light and reported as the average particle diameter, δ.

Transmission Electron Microscopy (TEM)

TEM Images of the lignin particles were taken using a FEI Talos F200X Transmission Electron Microscope (TEM). These samples were prepared by dropping a small amount of each suspension on a TEM grid and dried overnight.

Results and Discussion

Lignin Fractionation and Molecular Weight Distribution

It has been previously established that KL has different solubilities in various organic solvents due to the polarity of the solvent and hydrogen-bonding capability between the KL and the solvent.[13,36] Lignin has been shown to be successfully fractionated either with organic solvent/water mixtures[21,24,25] or using separate anhydrous organic solvents.[13,36] The characterization of KL fractions separated with three, water-miscible, anhydrous organic solvents directly used for particle precipitation has yet to be completed and is provided herein.

Fig. 4 includes the yields of KL in each fraction from solvent fractionation. KL was first dissolved in ethanol. The ethanol-insoluble portion was then dissolved in acetone. The remaining acetone-insoluble lignin was then dissolved in THF (see Fig. 3). Only 31.2% of KL was soluble in ethanol (E-Frac). Acetone was able to dissolve 54.7% of the ethanol-insoluble portion, corresponding to 37.6% of total KL mass (A-Frac). THF was able to dissolve 90.1% of the remaining KL, corresponding to 28.1% of the total KL mass (T-Frac). Directly mixing the original KL in acetone resulted in a solubility yield of 69.9% (AE-Frac). Finally, directly mixing the original KL with THF resulted in the dissolution of 96.9% of the entire KL sample (TAE-Frac).

In Fig. 5**,** the molecular weight distribution curves of each KL fraction acquired through GPC are shown. Table 1 contains the calculated number average (M_n) and weight average (M_w) molecular weight of each fraction from the distribution curves. In GPC, higher molecular weight (MW) species are too large to become entrapped within the pores of the column and elute first while the smaller MW species are entrapped within the small pores of the column and elute last (Fig. 5). When KL was fractionated, the low MW fractions reside in the ethanol solution (E-Frac), the intermediate MW fractions reside in the acetone solution (A-Frac), and only highest MW fractions of KL were solubilized in the THF solution (T-Frac), as evidenced in Fig. 5 and Table 1.

The combined KL fractions, TAE-Frac and AE-Frac, have much broader MW distributions compared to the individual fractions, as evidenced in Fig. 5 and Table 1. The AE-Frac MW distribution curve is representative of a mixture of the A-Frac and E-Frac, as expected. The TAE-Frac MW distribution contains all three of the individual lignin fractions (see Fig. 5). Solvents that result in a lower solubility of the KL sample, such as ethanol, can dissolve only the lower MW fractions, whereas the solvents that can dissolve higher MW fractions, such as THF and acetone, can also dissolve lower MW fractions. Reasons for this phenomenon are related to the chemical structure of the lignin fractions and will be discussed in the next section.

Table 1 Lignin fractionation results including molecular weight of each fraction after acetylation measured by gel-permeation chromatography (M_n: Number-average molecular weight; M_w: Weight-average molecular weight, PDI: polydispersity index).

Fraction	M_n (Da)	M_w (Da)	M_w/M_n (PDI)
TAE-Frac	1200	5600	4.66
AE-Frac	1200	3400	2.83
E-Frac	800	1400	1.75
A-Frac	1600	4000	2.5
T-Frac	5500	13000	2.36

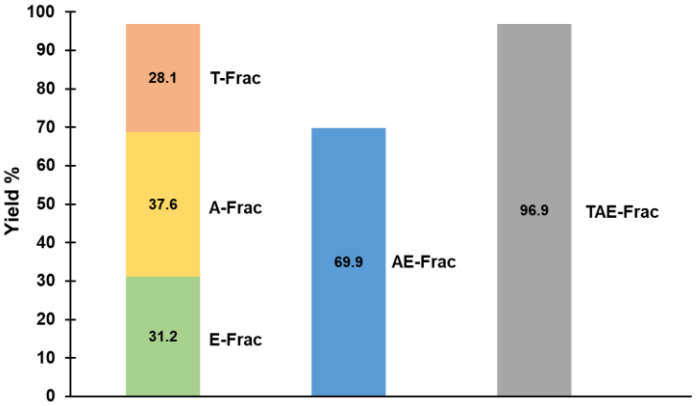

Fig. 4 Percentage yield of KL distributed in each fraction by mass percent. The first column (left) represents the completely separated fractions of KL extracted through solvent fractionation. The middle and right columns are representative of combined lignin fractions by dissolving KL in acetone (AE-Frac) and THF (TAE-Frac), respectively.

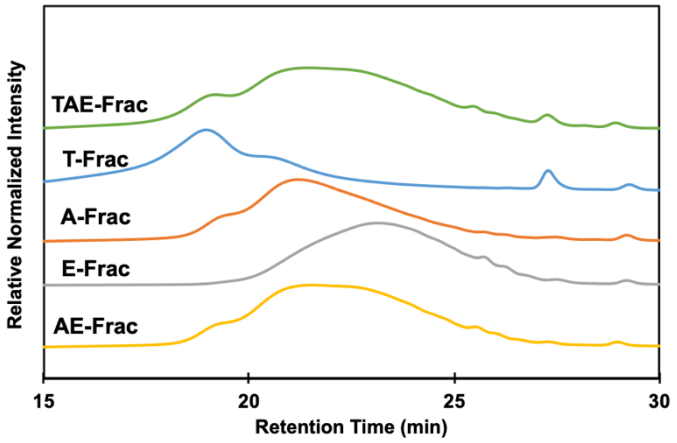

Fig. 5 Molecular weight distribution curves of each lignin fraction with the intensity normalized to 1 as measured by GPC. Higher molecular weight molecules elute first, whereas lower retention time corresponds to higher molecular weight.

NMR Analysis of Solvent Fractionated Kraft Lignin

Table 2 Hydroxyl content of kraft lignin fractions by ^{31}P NMR calculated as mmol/g of solid. The polarity of the organic solvent used to dissolve each fraction relative to water is listed as a reference value. C5-substitued-OH can be either 5-5 biphenyl structure or α-5 condensed G-unit. C5-free-OH contains a hydrogen in the C5 position. Finally, H-OH phenolic is the C5 and C3 free phenolic-OH.

Hydroxyl Group	TAE-Frac	AE-Frac	E-Frac	A-Frac	T-Frac
Aliphatic OH	1.93	1.41	1.41	1.51	2.04
Total Phenolic OH	**4.47**	**4.54**	**4.98**	**4.45**	**3.01**
C5-substituted-OH	1.98	1.93	2.03	2.08	1.48
C5-Free-OH	2.14	2.25	2.57	2.03	1.27
H-OH	0.36	0.35	0.38	0.34	0.26
COOH	0.62	0.62	0.60	0.51	0.37
Total OH	**7.03**	**6.30**	**6.99**	**6.47**	**5.42**
Solvent	THF	Acetone	Ethanol	Acetone	THF
Rel. Polarity of Solvent[37]	0.225	0.355	0.654	0.355	0.225
Boiling Point (°C)	66[38]	56[39]	78[40]	56[39]	66[38]

The solubility of KL fractions in organic solvents is dependent on the strength of interactions between the solute and solvent. For this reason, it was necessary to understand the chemical structure of the lignin fractions. ^{31}P NMR is a useful technique for identifying the hydroxyl content of lignins, which can then be related to the overall hydrophilicity or hydrophobicity of the sample. Table 2 describes the breakdown of hydroxyl groups present in each KL fraction.

In lignin, a higher hydroxyl content, notably phenolic hydroxyls, corresponds to higher hydrophilicity of the lignin molecule.[28] Due to their more acidic nature, the phenolic hydroxyl content (pKa~10) and carboxyl group (pKa~4) content will contribute more to the overall hydrophilicity of KL than the aliphatic hydroxyl groups (pKa~17).[41] Table 2 illustrates that ethanol is only able to dissolve the most hydrophilic lignin species (E-Frac), as evidence by the higher total hydroxyl content, whereas acetone soluble lignin fractions contain intermediate hydrophilicity (A-Frac) as well as high hydrophilic fractions (AE-Frac). THF can dissolve all KL species (TAE-Frac), including the most hydrophobic fractions (T-Frac) present in the sample (see Table 2). The higher polarity of the solvent precludes the dissolution of only more hydrophobic KL fractions, whereas lower polarity solvents (THF) are less selective in which KL fractions they may dissolve. This is due to the overall hydrophobic nature of KL, derived from its aromatic character.[28] While KL contains hydrophilic moieties, such as hydroxyl or carboxyl groups, the non-polarity of the KL remains significant.

Combining the results from both GPC and NMR analysis, a few conclusions can be made. First, KL can be fractionated using different organic solvents of varying polarity. More importantly, a smaller MW KL fraction, such as E-Frac, is related to a more hydrophilic character. In contrast, a larger molecular weight fraction, such as T-Frac, is related to a more hydrophobic character, (see Fig. 6). High polarity water-miscible solvents limits dissolution to lower MW, more hydrophilic lignin fractions, whereas lower polarity water-miscible solvents are less selective. These results are important when precipitating KL in a highly polar antisolvent such as water. In virtue of green chemistry principles and commercial scale-up of LP synthesis, acetone has the advantages for processing lignin due to the lower boiling point compared to ethanol and relatively low toxicity compared to THF.

Fractionation Effects on Lignin Particle Formation

The precursor soluble lignin fractions can be precipitated quickly into colloidal suspensions using water as an excess antisolvent. The effect of the KL fraction's chemical structure and molecular weight distribution on particle formation and colloidal behavior in aqueous suspensions is described here.

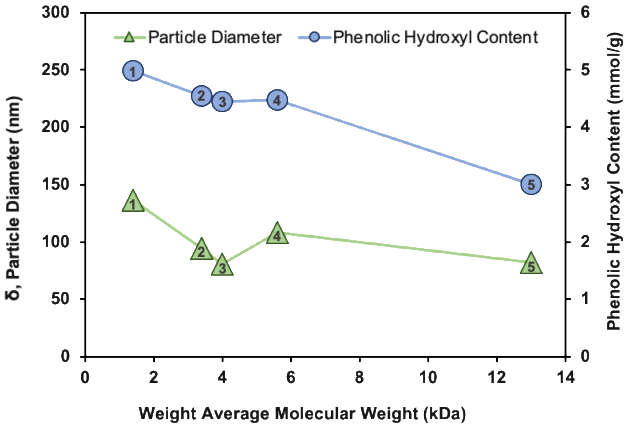

Fig. 6 Average particle diameter (δ), weight average MW, and phenolic hydroxyl content for 1) E-LPs, 2) AE-LPs, 3) A-LPs, 4) TAE-LPs, and 5) T-LPs at a precursor lignin solution concentration of 5 g/L. Error bars are smaller than the size of the icons. Standard deviation of particle diameters were < 10 nm.

The relationship between the average particle diameter (δ) measured using DLS, MW, and phenolic hydroxyl content for each lignin fraction is presented in Fig. 6. The LPs were precipitated from a precursor lignin concentration of 5 g/L. The phenolic hydroxyl content is reported in Fig. 6 rather than the total hydroxyl content because it is more likely representative of the overall hydrophilicity/hydrophobicity of the lignin fractions.[28]

Comparing the DLS results for fractionated KL samples, E-LPs have the largest δ (136 nm) and lowest average MW, whereas A-LPs (81 nm) and T-LPs (82 nm) are significantly smaller at a given lignin concentration despite having a higher average MW (Fig. 6). The LPs formed from the combined lignin fractions, TAE-LPs (108 nm) and AE-LPS (95 nm), exhibit an intermediate δ and phenolic hydroxyl contents relative to the particles formed from the individual lignin fractions that constitute them. The phenolic hydroxyl content and δ follow very similar trends with increasing weight-average MW of the KL fractions, indicating both the chemical composition/hydrophilicity and the MW of lignin molecules contribute to the nucleation and growth of the LPs.

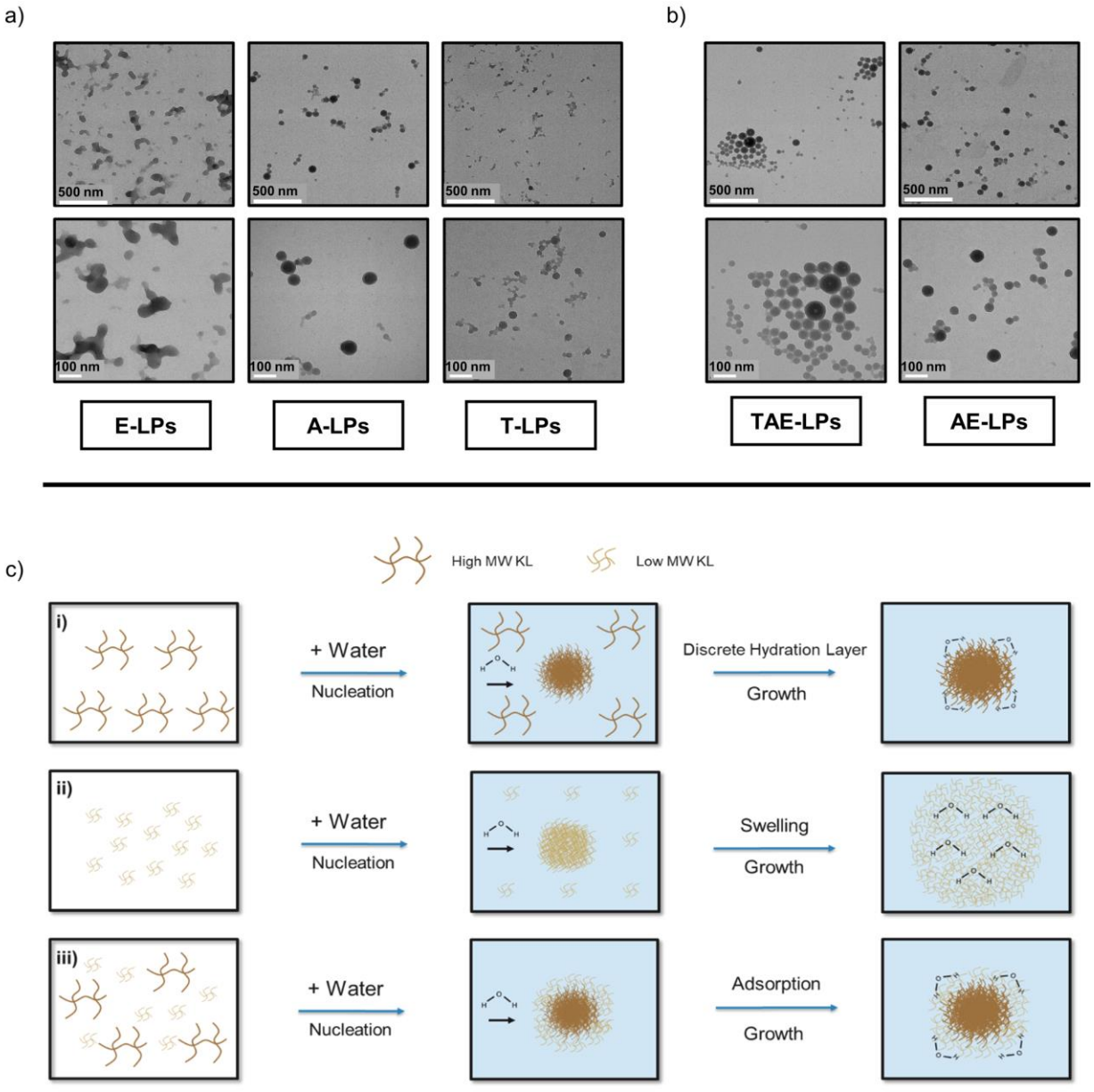

Fig. 7 a) TEM images of E-LPs, A-LPs, and T-LPs formed from the three separate lignin fractions, E-Frac, A-Frac, and T-Frac at an initial lignin concentration of 5 g/L. b) TEM images of AE-LPs and TAE-LPs formed from the combined lignin fractions, AE-Frac and TAE-Frac. c) Proposed mechanism of lignin particle nucleation and particle swelling. i) T-LP and A-LP nucleation of higher MW species followed by adsorption particle growth. ii) E-LP nucleation followed by adsorptive growth and particle swelling by means of osmosis. iii) TAE-LP and AE-LP nucleation of high MW lignin followed by particle growth by adsorption of lower MW lignin. Top row of TEM images scale bars = 500 nm and bottom row of TEM images = 100 nm.

Since DLS measures the hydrodynamic radius of particles in an aqueous medium, the particle diameters reported do not reflect particle shape. Thus, it was necessary to image the particle shape/morphologies using TEM. The TEM images for the individual lignin fractions and combined lignin fractions are shown in Fig. 7a-b. The TEM images can help explain the discrepancies in δ between each lignin fraction.

The terminology related to the interactions and destabilization of colloidal particles is often misused and should be properly defined in the context of this work. Particle aggregation (or agglomeration) is the adherence of individual particles with discrete particle boundaries and is typically a reversible process.[42] Conversely, coalescence and Ostwald ripening are irreversible processes that result in the disappearance of particle boundaries for the purpose of minimizing surface free energies, stabilizing otherwise unstable lyophobic particles.[43,44] However, coalescence and Ostwald ripening differ in their mass transfer mechanism. Coalescence occurs once unstable particles have collided, whereas Ostwald ripening involves the dissolution of surface-present molecules of smaller particles and the subsequent adsorption of such molecules on larger particles.[43,44] It is worth noting a more hydrophilic particle favors Ostwald ripening in aqueous systems, due to greater solubility.[45] In the case of LPs it is difficult to distinguish for certain whether Ostwald ripening or coalescence is the mode of action, therefore the two terms will be hereby referred to as particle fusion.

As shown in Fig. 7a, A-LPs have a well-developed spherical morphology, with similar homogeneity and size as reported elsewhere.[22,24,46] In the case of T-LPs, the particles appear to be much smaller than A-LPs as evidenced by TEM imaging (Fig. 7a), yet the DLS results report very similar δ's, 82 nm and 81 nm respectively (see Fig. 6). This could likely be due to the increased degree of aggregation and particle fusion present in the T-LP sample compared to A-LPs. These larger aggregates resemble diameters similar to the A-LPs (see Fig. 7a).

The smaller individual particle sizes of T-LPs depicted in Fig. 7a is perhaps due to the more hydrophobic character. The higher hydrophobicity leads to a lower supersaturation concentration, thus favoring nucleation over growth, yielding a large number of smaller particles.[47,48] The increased propensity for T-LPs to fuse and aggregate can be attributed to the higher hydrophobicity. Hydrophobicity at the nanoscale increases the degree of entropic aggregation, as described by the hydrophobic effect, as well as the tendency to reduce the overall surface free energy in aqueous suspensions.[34,49] The reduction of surface free energy by particle fusion will be discussed further in the next section.

In the case of E-LPs, the TEM images suggest the more hydrophilic lignin fractions form soft, metastable, semi-solid particles in the aqueous medium (see Fig. 7a). These particles will readily deform and fuse upon collisions with other particles. The lack of hydrophobic forces necessary for phase separation can lead to diffusion of water into the particle structure (particle swelling) and deformation of the LP.

The LPs formed from the combined lignin fractions, TAE-LPs and AE-LPS, may elucidate the effect of MW and MW distribution on particle size. The TEM images in Fig. 7b suggest the TAE-LPs have a larger particle size distribution and δ than AE-LPs. This can be attributed to the higher polydispersity of TAE-Frac compared to AE-Frac. Kinetically, since nucleation is highly dependent on the supersaturation condition, the nucleation of hydrophobic, high MW lignin molecules rapidly reduces the concentration of supersaturated lignin molecules. This results in a larger population of lower MW lignin molecules involved in particle growth.[48,50] This rationale is consistent when comparing the δ and TEM images of A-LPs and AE-LPs. In this comparison, the lignin molecules that form the initial nuclei are composed of the same MW and chemical compostion, following the aforementioned nucleation mechanism. Therefore, given the same lignin mass, the AE-LPs will contain less lignin molecules that can participate in a nucleation and more lignin molecules that will participate in growth. Thus, greater polydispersity in the lignin sample will lead to less nucleation and more growth.

Fig. 7c illustrates the proposed particle swelling mechanism of LPs. Two cases are depicted in Fig. 7c: i) the more hydrophobic, high MW fractions of KL, represented by T-Frac and A-Frac, nucleate and grow into compact hydrophobic particles, ii) the particles formed from the more hydrophilic, low MW fractions of KL swell by osmosis through the particle's surface, driven by stronger interactions of the lignin species with water, representative of E- LPs, and iii) the particles formed from the combined lignin fractions, TAE-Frac and AE-Frac, first nucleate the high MW lignin species, followed by the adsorption of lower MW lignin species on the particle surface, resulting in a compact hydrophobic core, surrounded by a more hydrophilic shell. This swelling mechanism can be supported by previous studies in which the porosity of lignin was investigated indirectly, where LPs were found to be penetrable by water and water-soluble molecules.[21,51,52]

Overall, there seems to be a trade-off between the MW distribution and chemical composition of the lignin fractions with respect to resulting particle size and aggregation/fusion propensity. The chemical composition of the lignin fractions used for nanoprecipitation affects the hydrophobicity of the LPs. This hydrophobicity can be related to differences in the nucleation and growth kinetics, particle aggregation/fusion, and particle metastability through partial dissolution in aqueous suspensions upon particle collision and/or close proximities. Previous studies have found aromatic interactions to be a significant contributor to particle formation.[30,53] These non-DLVO interactions between particles are possible but the steric strain present between spherical structures will likely prevent these close-range interactions from becoming significant. Although, it is possible π-π interactions will contribute to the particle growth via coalescence/ripening once particles come into contact. The average particle size reported from DLS is less useful than TEM when comparing the actual morphologies of resulting lignin particles from nanoprecipitation. TEM imaging suggests that particle aggregation/fusion, hydrophobic forces, and surface free energies of lignin particles must be considered.

Concentration Effects on Lignin Particle Formation

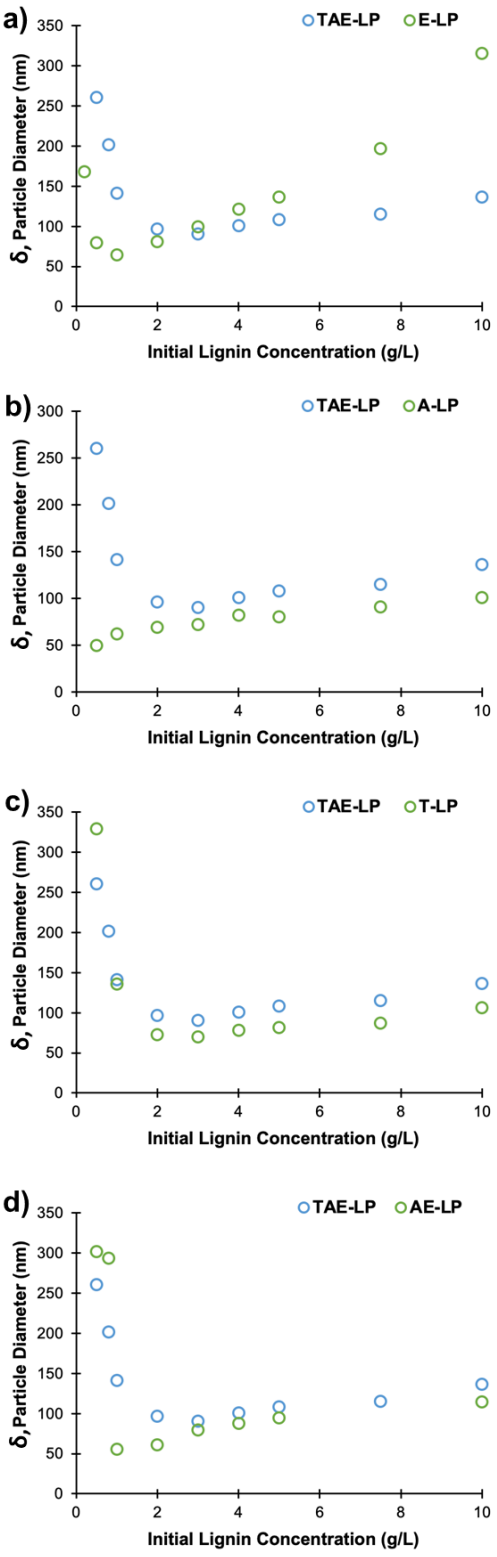

Fig. 8 Average particle diameter as a function of precursor lignin concentration for TAE-LPs, E-LPs, A-LPs, T-LPs, and AE-LPs as determined by DLS. TAE-LPs are plotted along with the other LP samples for comparison of the average particle diameter over the concentration profiles. Error bars are smaller than the size of the icons. Standard deviation of particle diameters were < 10 nm.

The size of the LPs measured with DLS was investigated as a function of the dissolved lignin concentration (i. e, initial lignin concentration) for each of the lignin fractions. In general, as the initial lignin concentration decreases, the particle diameter decreases as well in the linear region (see Fig. 8). The general trend can be attributed to less lignin molecules present per unit volume participating in nucleation and growth. The lignin particles likely follow the nucleation and growth mechanism proposed by La Mer et al.[50] This mechanism involves the burst nucleation of supersaturated hydrophobic molecules yielding a constant number of nuclei at a minimum particle size.[23,48,50] The supersaturation condition necessary for burst nucleation quickly subsides after the precipitation of suspended particles. The excess lignin molecules not involved in nucleation possess a very high surface energy in the aqueous medium from their overall hydrophobic character, and readily adsorb to the formed lignin nuclei.[48,50] The increase in size with increasing lignin concentration is due to the growth of the particles via adsorption of lignin molecules to the initially formed nuclei.

However, when the initial lignin concentration is reduced significantly, the apparent particle diameters measured via DLS are much larger after precipitation, as evidenced by Fig. 8. This phenomenon has also been observed in similar studies.[22,23,48] The concentration at which this occurs can be referred to as the critical concentration, C_0. This phenomenon is consistent for each lignin fraction in the concentration ranges studied, with the exception of A-LPs, but occurs at different concentrations of lignin in solution. The C_0 is the highest in T-LPs and TAE-LPs and lowest with E-LPs and AE-LPs (Table 3). A-LPs did not exhibit a C_0 from the concentrations measured (0.5 – 10 g/L).

Table 3 Critical initial lignin concentration (C_0) and resulting average particle diameters measured by DLS for each solvent system.

	C_0 (g/L)	Particle Diameter (nm)
TAE-LP	3.0	90
E-LP	1.0	65
A-LP	N/A	50
T-LP	3.0	70
AE-LP	1.0	56

This phenomenon can be further exemplified by Fig. 9, where the particle size distribution of T-LPs, measured by DLS, above and below C_0 is depicted. For T-LPs, C_0 was 3 g/L, where initial lignin concentrations below C_0 result in the appearance of a peak at much larger particle sizes (~10x). As the precursor lignin concentration is reduced below C_0, the first peak (left), representative of dispersed individual particles, decreases in intensity and shifts left, indicating smaller particle sizes, but at a lower abundance. The second peak (right) increases in intensity dramatically as the first peak is reduced, indicating the presence of either fusion or aggregation of individual particles.

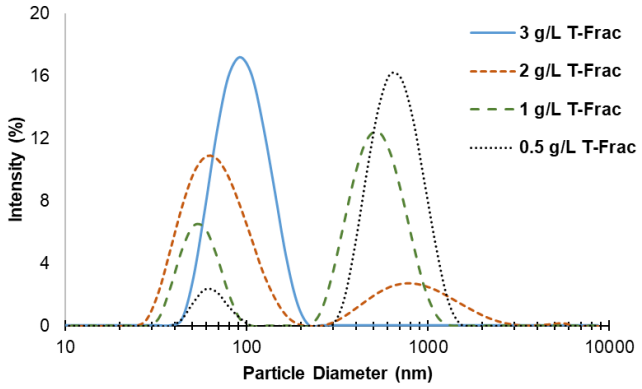

Fig. 9 Scattered light intensity weighted particle size distribution of T-LPs approaching the critical concentration, C_0, measured by DLS

TEM images were taken for T-LPs fabricated at initial lignin concentrations above and below C_0 (5 g/L and 1 g/L, respectively). The TEM images are reported in Fig. 10.

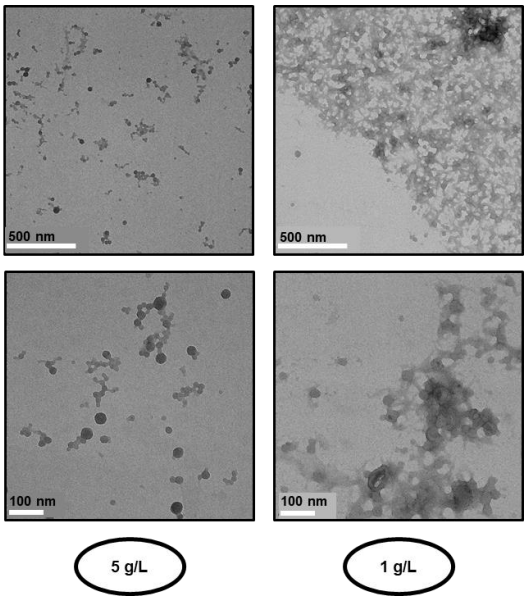

Fig. 10 TEM images of T-LPs at an intial lignin concentration of 5 g/L and 1 g/L in THF prior to antisolvent addition.

The TEM images suggests extensive aggregation and fusion of the particles at lower lignin concentrations in order to maximize their thermodynamic stability.[54,55] When the lignin concentration is reduced significantly, the particles formed are much smaller, resulting in a very large surface area to volume ratio (S/V, Eq. 4), where R is the particle radius.

$$\frac{Surface\ Area}{Volume} = \frac{4\pi R^2}{\left(\frac{4}{3}\right)\pi R^3} = \frac{3}{R} \quad (4)$$

Smaller, charged particles, will have a favorable charge-to-mass ratio over larger particles, normally improving colloidal stability. Although, when surface charge remains constant and particle size decreases, DLVO theory dictates a lower electrostatic repulsive barrier (Fig. 11).[56] The high S/V ratio in a lyophobic suspension can give rise to a high overall surface free energy, eventually leading to particle aggregation and fusion, as determined by the Lifshitz-Slyozov-Wagner (LSW) theory.[49,55,57–59] In theory, given enough time, all particles of like-materials will eventually form one large particle containing the entire mass of the sample. Although, repulsive forces help resist this tendency for all particles to completely fuse. Therefore, the stability of the LPs is determined by the trade-off between electrostatic repulsive forces and surface free energy. The lignin particles formed below C_0 will be highly unstable and quickly aggregate and fuse upon collisions with nearby larger particles (see Fig. 10). This process enhances the overall thermodynamic stability of the suspension, where the surface free energy is more favorable for larger particles.[55,60]

A kinetic reasoning for larger particle size can also be proposed following the previously described mechanism proposed by La Mer et al.[50] As the lignin concentration drops below C_0 the supersaturation condition is reduced as well. Thus, the amount of lignin that is involved in nucleation is much less given that the nucleation rate is mostly dependent on the degree of supersaturation.[47,48,54] Therefore, growth is favored or nucleation. Although this may contribute to an overall larger particle size, the TEM images suggest interparticle attraction and particle fusion are the dominating factors driving the sudden gain in apparent particle diameter measured by DLS (see Fig. 10).

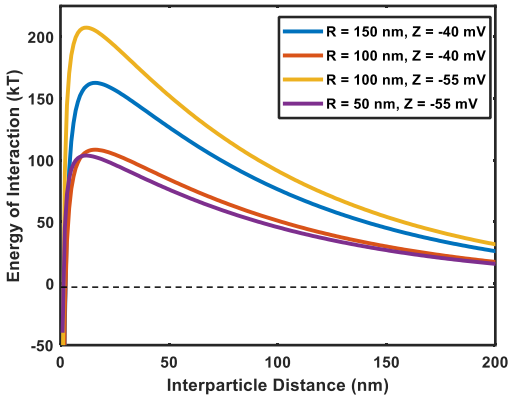

Fig. 11 Energy of interactions between lignin particles following DLVO model including electrostatic and Van der Waals interactions. Input parameters are shown in the figure legend. Hamaker constant = 1.7 x 10^{21} J, Ionic strength = 0.001 M, ε = 78.5, κ^{-1} = 10 nm.

The proposed LP aggregation/fusion mechanism at low lignin concentration would also explain why the more hydrophobic particles (T-LP, TAE-LPs) have a higher C_0 than the other more hydrophilic particles (see Table 3). The more hydrophilic particles will likely have a lower surface free energy due to the increased content of hydroxyl groups present on the surface of the particles (Table 2). Interestingly, A-LPs did not exhibit a significant increase in particle size from a reduction of lignin concentration while the more hydrophilic E-LPs exhibited extensive particle size increases (~150%). This could be the

result of the E-LPs "soft" particle morphology due to particle swelling, where there is a lack of a discrete repulsive electrostatic double layer.[25] The A-LPs exhibited the best overall particle characteristics with respect to small size, morphology, stability and homogeneity, derived from the ability to form a discrete, compact hydrophobic core while still containing enough hydrophilic groups to minimize surface energy.

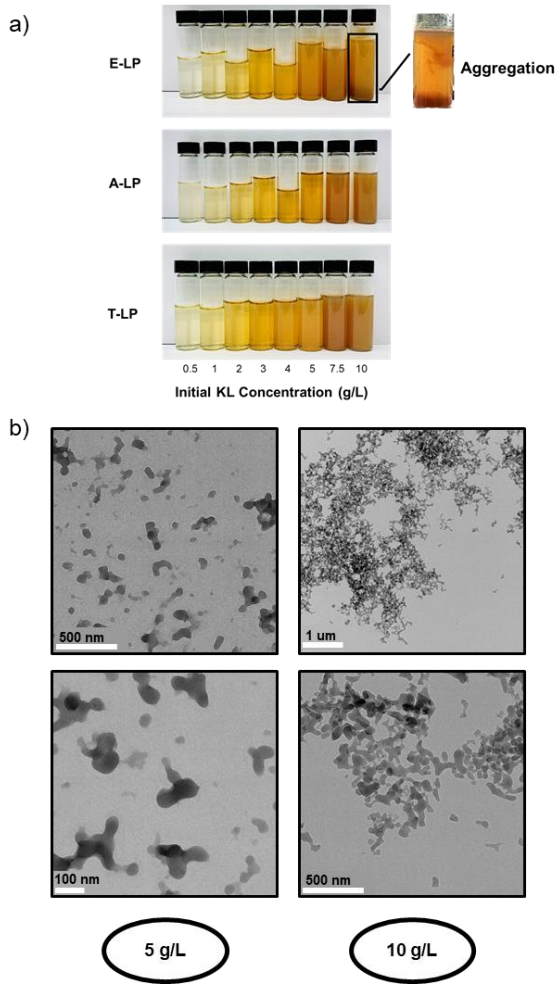

Fig. 12 a) Lignin particle suspensions with increasing precursor lignin concentration for each of the separated fractions. All suspensions seemed visibly well-dispersed with the exception of E-LPs at 7.5 and 10 g/L where sedimentation and flocculation is visible. b) TEM images of E-LPs at an initial lignin concentration of 5 g/L and 10 g/L in solution prior to antisolvent addition.

It appears that the LPs are well dispersed at higher concentrations for samples including T-LPs and A-LPs but aggregate to the point of visible sedimentation at initial lignin concentrations above 5 g/L for E-LPs (see Fig. 12a). The extensive aggregation was also observed by TEM imaging (Fig. 12b). As already mentioned, as the content of hydrophilic groups present in the lignin fraction is higher, such that as the case for E-LPs, possible particle swelling could lead to the formation of soft, metastable particles.[13,24] This metastability could stem from the reduction of the hydrophobic forces necessary for complete particle phase separation and stability. As the concentration becomes greater, the interparticle distances will decrease significantly, where the metastability can lead to aggregation. The formation of LPs with more hydrophobic behavior remain stable at higher lignin concentrations.

Conclusions

Synthesis of lignin particles via nanoprecipitation has improved significantly in the past years with respect to the spherical morphology, homogeneity, and colloidal stability. The results shown in this work suggest more is to be understood about the effects of chemical composition, MW, particle aggregation/fusion propensity, and metastability of LPs.

It was determined that water-miscible organic solvents can be used to effectively fractionate KL into three distinct fractions, each with a unique set of chemical and physical properties. Each of the separate lignin fractions contained roughly 30% of the total KL sample, resulting in an even distribution of the starting KL molecules. It was determined that as the polarity of the solvent increases, the soluble lignin fraction is more hydrophilic. The hydrophilic character of the lignin fraction used likely attributes to particle swelling with water and colloidal metastability. Increased hydrophobicity of lignin also exhibited higher degrees of aggregation of individual particles. Additionally, a mechanism was proposed relating to particle aggregation/fusion and metastability of LPs at low precursor lignin concentrations.

These results enable a deeper understanding to the factors attributing to lignin particle synthesis via a solvent shifting method, further elucidating the effect of solvent-lignin-antisolvent interactions, and lignin concentration. In virtue of the application or scale-up of colloidal lignin particle synthesis, the effects of organic solvents may become significant with respect to green chemistry principles, cost, particle stability, and biocompatibility. It was concluded that the particle formed from A-Frac is most likely the best option from the solvents studied for the solvent shifting process, when homogeneity, small size, and morphology are of interest. This is due to the favorable equilibrium between the hydrophobicity and hydrophilicity of the lignin fraction leading to a relatively low surface free energy but also a compact hydrophobic core when transformed into a spherical nanoparticle. Additionally, when considering green chemistry principles, acetone will allow for a lower energy demand during solvent removal compared to ethanol, as well as lower toxicity and hazards typically associated with THF.

Conflicts of interest

There are no conflicts to declare

Acknowledgements

The project is supported by the USDA-NIFA grant:12513354, and AFRI Competitive Grants Program: Sustainable Bioenergy

and Bioproducts Challenge Area: Investing in America's Scientific Corps: Preparing a New Generation of Students, Faculty, and Workforce for Emerging Challenges in Bioenergy, Bioproducts, and the Bioeconomy, award number: 2017-67009-26771, Program Code - A6131.

Notes and references

1 A. Duval and M. Lawoko, *React. Funct. Polym.*, 2014, **85**, 78–96.
2 G. Gellerstedt and G. Henriksson, *Business*.
3 Z. Hu, X. Du, J. Liu, H. M. Chang and H. Jameel, *J. Wood Chem. Technol.*, 2016, **36**, 432–446.
4 F. S. Chakar and A. J. Ragauskas, 2004, **20**, 131–141.
5 S. R. Yearla and K. Padmasree, *J. Exp. Nanosci.*, 2016, **11**, 289–302.
6 Y. Qian, X. Qiu and S. Zhu, *Green Chem.*, 2015, **17**, 320–324.
7 T. E. Nypelö, C. A. Carrillo and O. J. Rojas, *Soft Matter*, 2015, **11**, 2046–2054.
8 X. Guo, S. Zhang and X. quan Shan, *J. Hazard. Mater.*, 2008, **151**, 134–142.
9 A. P. Richter, J. S. Brown, B. Bharti, A. Wang, S. Gangwal, K. Houck, E. A. Cohen Hubal, V. N. Paunov, S. D. Stoyanov and O. D. Velev, *Nat. Nanotechnol.*, 2015, **10**, 817–823.
10 W. Yang, J. S. Owczarek, E. Fortunati, M. Kozanecki, A. Mazzaglia, G. M. Balestra, J. M. Kenny, L. Torre and D. Puglia, *Ind. Crops Prod.*, 2016, **94**, 800–811.
11 D. Kun and B. Pukánszky, *Eur. Polym. J.*, 2017, **93**, 618–641.
12 X. Jiang, J. Liu, X. Du, Z. Hu, H. M. Chang and H. Jameel, *ACS Sustain. Chem. Eng.*, 2018, **6**, 5504–5512.
13 X. Jiang, D. Savithri, X. Du, S. Pawar, H. Jameel, H. M. Chang and X. Zhou, *ACS Sustain. Chem. Eng.*, 2017, **5**, 835–842.
14 O. U. Rahman, S. Shi, J. Ding, D. Wang, S. Ahmad and H. Yu, *New J. Chem.*, 2018, **42**, 3415–3425.
15 C. Jiang, H. He, H. Jiang, L. Ma and D. M. Jia, *Express Polym. Lett.*, 2013, **7**, 480–493.
16 T. Kämäräinen, M. Ago, J. Seitsonen, J. Raula, E. I. Kauppinen, J. Ruokolainen and O. J. Rojas, *Soft Matter*, 2018, **14**, 3387–3396.
17 M. Österberg, M. H. Sipponen, B. D. Mattos and O. J. Rojas, *Green Chem.*, , DOI:10.1039/d0gc00096e.
18 S. Beisl, A. Friedl and A. Miltner, *Lignin from micro- To nanosize: Production Methods*, 2017, vol. 18.
19 B. L. Tardy, J. J. Richardson, J. Guo, J. Lehtonen, M. Ago and O. J. Rojas, *Green Chem.*, 2018, **20**, 1335–1344.
20 T. Leskinen, M. Smyth, Y. Xiao, K. Lintinen, M.-L. Mattinen, M. A. Kostiainen, P. Oinas and M. Österberg, *Nord. Pulp Pap. Res. J.*, 2017, **32**, 586–596.
21 M. H. Sipponen, H. Lange, M. Ago and C. Crestini, *ACS Sustain. Chem. Eng.*, 2018, **6**, 9342–9351.
22 A. P. Richter, B. Bharti, H. B. Armstrong, J. S. Brown, D. Plemmons, V. N. Paunov, S. D. Stoyanov and O. D. Velev, *Langmuir*, 2016, **32**, 6468–6477.
23 M. Lievonen, J. J. Valle-Delgado, M. L. Mattinen, E. L. Hult, K. Lintinen, M. A. Kostiainen, A. Paananen, G. R. Szilvay, H. Setälä and M. Österberg, *Green Chem.*, 2016, **18**, 1416–1422.
24 M. Ma, L. Dai, J. Xu, Z. Liu and Y. Ni, *Green Chem.*, 2020, **22**, 2011–2017.
25 T. Leskinen, M. Smyth, Y. Xiao, K. Lintinen, M. L. Mattinen, M. A. Kostiainen, P. Oinas and M. Österberg, *Nord. Pulp Pap. Res. J.*, 2017, **32**, 586–596.
26 W. Zhao, B. Simmons, S. Singh, A. Ragauskas and G. Cheng, *Green Chem.*, 2016, 18, 5693–5700.
27 M. Ago, B. L. Tardy, L. Wang, J. Guo, A. Khakalo and O. J. Rojas, *MRS Bull.*, 2017, **42**, 371–378.
28 J. Wang, Y. Qian, L. Li and X. Qiu, *ChemSusChem*, 2020, 1–9.
29 T. Pang, G. Wang, H. Sun, L. Wang, Q. Liu, W. Sui, A. M. Parvez and C. Si, *ACS Sustain. Chem. Eng.*, 2020, **8**, 9174–9183.
30 I. V. Pylypchuk, P. A. Lindén, M. E. Lindström and O. Sevastyanova, *ACS Sustain. Chem. Eng.*, 2020, **8**, 13805–13812.
31 W. G. Glasser, V. Davé and C. E. Frazier, *J. Wood Chem. Technol.*, 1993, **13**, 545–559.
32 D. S. Argyropoulos, *J. Wood Chem. Technol.*, 1994, **14**, 45–63.
33 A. Granata and D. S. Argyropoulos, *J. Agric. Food Chem.*, 1995, **43**, 1538–1544.
34 J. Israelachvili, *Intermolecular and Surface Forces*, 2011.
35 R. Hollertz, H. Arwin, B. Faure, Y. Zhang, L. Bergström and L. Wågberg, *Cellulose*, 2013, **20**, 1639–1648.
36 C. Schuerch, *J. Am. Chem. Soc.*, 1952, **74**, 5061–5067.
37 C. Reichardt and T. Welton, *Solvents and Solvent Effects in Organic Chemistry: Fourth Edition*, 2010.
38 National Center for Biotechnology Information, PubChem Compound Summary for CID 8028, Tetrahydrofuran, https://pubchem.ncbi.nlm.nih.gov/compound/Tetrahydrofuran., (accessed 8 September 2020).
39 National Center for Biotechnology Information, PubChem Compound Summary for CID 180, Acetone, https://pubchem.ncbi.nlm.nih.gov/compound/Acetone., (accessed 8 September 2020).
40 National Center for Biotechnology Information, PubChem Compound Summary for CID 702, Ethanol.
41 M. Ragnar, C. T. Lindgren and N. O. Nilvebrant, *J. Wood Chem. Technol.*, 2000, **20**, 277–305.
42 S. Slomkowski, J. V. Alemán, R. G. Gilbert, M. Hess, K. Horie, R. G. Jones, P. Kubisa, I. Meisel, W. Mormann, S. Penczek and R. F. T. Stepto, *Pure Appl. Chem.*, 2011, **83**, 2229–2259.
43 *IUPAC Compend. Chem. Terminol.*, 2008, **577**, 2014.
44 *IUPAC Compend. Chem. Terminol.*, 2008, **1801**, 4348.
45 E. Lepeltier, C. Bourgaux and P. Couvreur, *Adv. Drug Deliv. Rev.*, 2014, **71**, 86–97.
46 H. Setälä, H. L. Alakomi, A. Paananen, G. R. Szilvay, M. Kellock, M. Lievonen, V. Liljeström, E. L. Hult, K. Lintinen, M. Österberg and M. Kostiainen, *Cellulose*, 2019, **9**, 273–284.
47 W. S. Saad and R. K. Prud'Homme, *Nano Today*, 2016, **11**, 212–227.
48 C. Destrée and J. B.Nagy, *Adv. Colloid Interface Sci.*, 2006, **123–126**, 353–367.

49 P. Dagtepe and V. Chikan, *J. Phys. Chem. C*, 2010, **114**, 16263–16269.
50 V. K. Lamer and R. H. Dinegar, *J. Am. Chem. Soc.*, 1950, **72**, 4847–4854.
51 L. Dai, R. Liu, L. Q. Hu, Z. F. Zou and C. L. Si, *ACS Sustain. Chem. Eng.*, 2017, **5**, 8241–8249.
52 Y. Qian, L. Lü, X. Qiu, Y. Deng, H. Zhao and B. Wang, *Ind. Crops Prod.*, 2016, **87**, 191–197.
53 P. K. Mishra and A. Ekielski, *Nanomaterials*, 2019, **9**, 243.
54 N. T. K. Thanh, N. Maclean and S. Mahiddine, *Chem. Rev.*, 2014, **114**, 7610–7630.
55 L. Ratke and P. W. Voorhees, *Choice Rev. Online*, 2002, 117–118.
56 L. M. Liz-Marzán, M. A. Correa-Duarte, I. Pastoriza-Santos, P. Mulvaney, T. Ung, M. Giersig and N. A. Kotov, *Handb. Surfaces Interfaces Mater.*, 2001, **3**, 189–237.
57 J. A. Marqusee and J. Ross, *J. Chem. Phys.*, 1984, **80**, 536–543.
58 D. V. Talapin, A. L. Rogach, M. Haase and H. Weller, *J. Phys. Chem. B*, 2001, **105**, 12278–12285.
59 I. M. Lifshitz and V. V. Slyzov, *Phys. Chem. Solids*, 1961, **19**, 35–50.
60 C. Ribeiro, E. J. H. Lee, E. Longo and E. R. Leite, *ChemPhysChem*, 2005, **6**, 690–696.